Rice Autonomous Harvesting: Operation Framework

Hiroki Kurita
Department of Electrical and Electronic Engineering, Ritsumeikan University, Kusatsu, Japan
e-mail: kuritahrikc@gmail.com
Michihisa Iida
Division of Environmental Science and Technology, Kyoto University, Kyoto, Japan
e-mail: iida@elam.kais.kyoto-u.ac.jp
Wonjae Cho
Institute of Agricultural Machinery, NARO, Ibaraki, Japan
e-mail: chou555@affrc.go.jp
Masahiko Suguri
Division of Environmental Science and Technology, Kyoto University, Kyoto, Japan
e-mail: suguri@elam.kais.kyoto-u.ac.jp

Received 15 March 2014; accepted 21 October 2016

This paper reports on an operation framework for autonomous rice harvesting. We developed an integrated algorithm for robotic operation and cooperation with farmworkers to automate each subsection of the harvesting and unloading process and of the processes that bridge them (homing and restarting). The algorithm was installed into a head-feeding combine robot. The robot followed a target path based on its absolute position and orientation, planning a counterclockwise spiral path in a rectangular paddy field, and returned to a position close to a farm road when its grain tank was filled to a specified level. The grain unloading operation was automated using a machine vision system. As the restarting process (return to harvesting) was also automated, the combine robot was able to harvest a rectangular field autonomously by cyclically repeating the harvesting, homing, unloading, and restarting operations. Under field conditions, the robot was able to follow the target path within tolerable lateral and azimuth errors while harvesting rice successfully, and to unload the harvested grain into a wagon without spillage. The root mean square error of the lateral and azimuth errors during harvesting were 0.04 m and 2.6°, respectively. In the homing operation, the robot returned to a given line within ± 0.1 m and aligned its heading to the direction of the line within ± 4°. The robot recognized the arbitrarily parked wagon and positioned its auger spout at the target point with a respective horizontal and vertical accuracy of ± 0.2 m and ± 0.3 m. Harvesting time accounted for 50%–60% of the entire robotic operation. Homing scheduling and dispatch control for the wagon were found to be of importance for developing a more efficient robotic operation. © 2017 Wiley Periodicals, Inc.

1. INTRODUCTION

The automation of agricultural machinery is an ongoing challenge in the field of agricultural engineering. Accurate vehicle guidance, in particular, is of great importance to automation from tilling to harvesting. Various studies have been conducted into autonomous agricultural vehicle guidance (Keicher & Seufert, 2000; Reid, Zhang, Noguchi, & Dickson, 2000; Torii, 2000). Machine vision is widely used for autonomous guidance by detecting crop rows (Åstrand & Baerveldt, 2002; Billingsley & Schoenfisch, 1997; Han, Zhang, Ni, & Reid, 2004; Kise, Zhang, & Rovira-Más, 2005; Xue, Zhang, & Grift, 2012). Alternatively, a laser range finder (LRF) is commonly used (Barawid, Mizushima, Ishii, & Noguchi, 2007; Chateau, Debain, Collange, Trassoudaine, & Alizon, 2000), swath detection (Coen, Vanrenterghem, Saeys, & De Baerdemaeker, 2008), or obstacle avoidance (Kise, Zhang, & Noguchi, 2005). The method of sensor fusion has also been shown to be a promising technique for autonomous guidance (Subramanian, Burks, & Arroyo, 2006). Global navigation satellite systems (GNSS) have proven robust in detecting a vehicle's absolute position, and GNSS-guided prototypes have been reported: a forage harvester (Stoll & Kutzbach, 2000), a tractor for weed control (Nørremark, Griepentrog, Nielsen, & Søgaard, 2008), and a rice transplanter (Nagasaka et al., 2009; Nagasaka, Umeda, Kanetai, Taniwaki, & Sasaki, 2004) are a few examples. According to Wilson (2000), all approaches for autonomous guidance revert to two distinct modes: (1) guidance with respect to a directrix generated by the previous pass or operation, and (2) guidance with

Direct correspondence to: Hiroki Kurita; e-mail: kuritahrikc@gmail.com

respect to a directrix generated by fixed points in the field. Machine vision, LRF, or a combination of both, belongs to the first mode, while a GNSS-based system is classified in the second mode.

The automation of a combine harvester has been studied using both the first (Benson, Reid, & Zhang, 2003; Rovira-Más, Han, Wei, & Reid, 2007) and the second mode (Cordesses, Cariou, & Berducat, 2000). It was reported that a second mode system presents performance comparable to the first mode system in line tracking tasks including curves or circles, yet the first mode system has difficulty in dealing with other tasks in harvesting such as keeping a vehicle near the boundaries of a field, turning at headlands, and unloading the crop into a wagon. In harvesting, a human operator of a combine normally also has to unload the harvested crops into a wagon. In addition to autonomous guidance, autonomous unloading for forage harvesters has been studied (Happich, Harms, & Lang, 2009; Madsen, Kirk, & Blas, 2009). CLAAS commercializes harvesters with an AUTO FILL function. Their aim, however, is to construct an operator-assisted system, not an operator-free one. This is because the system is designed to be used in a large field and is required to unload crops into a parallel-traveling wagon while harvesting.

In summary, previous research on combine harvesters has focused primarily on guidance or, to a lesser extent, unloading. These aspects do not provide solutions for operator-free harvesting. More importantly, no one has as yet discussed the idea that a robot could perform the entire operation autonomously, and therefore no operation frameworks to realize this concept exist. When applying a combine robot to actual rice paddy fields, the robot must be included in a working system that also includes farmworkers. The objectives of this study are thus to present an operation framework for autonomous rice harvesting. This framework includes an integrated algorithm for autonomous operation and cooperation with farmworkers.

2. HUMAN OPERATION FRAMEWORK

2.1. Rice Harvesting in Japan

This section provides an overview of rice harvesting in Japan and describes the way it is conducted by farmers. Rice is a staple agricultural product in Japan. Figure 1 shows a typical layout of rice paddy fields in this country. They are enclosed by embankments about half a meter in width, since they are flood irrigated. The paddy will also border at least one road for access by agricultural machinery. In general, a Japanese paddy field is quite small and segmented in comparison to European or American fields, and thus relatively small machinery is used. The typical field size in Japan is 0.3 ha, which is similar to in Korea but relatively small compared to in Italy or California, roughly speaking, about 2 ha and 4 ha, respectively. Accordingly, the operator of a combine harvester is not required to follow a long straight path,

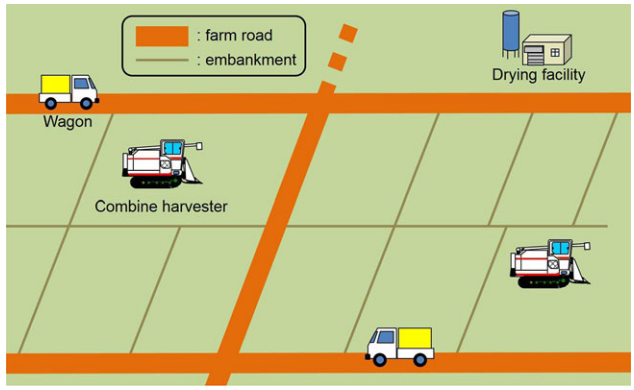

Figure 1. Conventional operation framework for rice harvesting in Japan. Each field is enclosed by an embankment and farm road. Some farmworkers operate combine harvesters and others drive wagons between fields and the drying facility.

but operation instead requires frequent turning at the end of crop rows and unloading the harvested grain into a wagon. The wagon remains at an appropriate point on the adjacent farm road while unloading. The driver then conveys the grain to a drying facility. Rice harvesting is thus a task performed cooperatively by the operator and the driver. Another distinct feature of Japanese paddy fields is their shape, as multiple irregular fields have now frequently consolidated into a rectangular shape of almost 30 m × 100 m. If a combine robot were developed to work in a field of this description, it could be expected to be applied to a large number of fields nationwide.

2.2. Previous Work

The project team at Kyoto University has been engaged in the development of an autonomous head-feeding combine harvester. They reported on the path following algorithm (Iida et al., 2013) and showed that their previously developed robot, VY50, showed sufficient path tracking performance. Their study, however, does not present a way of applying the algorithm to the entire process of harvesting. The robot harvested rice until its grain tank was full, at which point a human operator had to drive it to a position close to the farm road and manually unload the grain into a wagon. The operator also had to drive it to the remaining crop area to continue executing the robotic harvesting. The robot therefore needed to be handled by an operator occasionally, and thus remained an operator-assisted system.

A machine vision system (called "the auger camera system" in this study) was also presented for use in the autonomous unloading operation (Kurita, Iida, Suguri, & Masuda, 2012; Kurita, Iida, Suguri, Masuda, & Cho, 2014). Using this system, the robot can position its auger spout (the tip of the unloading auger) at a given target point over a wagon. This auger camera system, however, severely

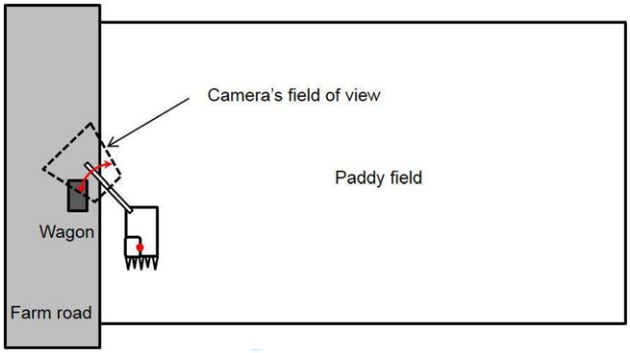

Figure 2. The auger camera system for grain unloading. The robot searches for the marker on the wagon roof at a predetermined position by rotating its unloading auger, to which a camera is fixed. Farmworkers must park the wagon at an appropriate predetermined position. The camera's field of view is represented with a trapezoid.

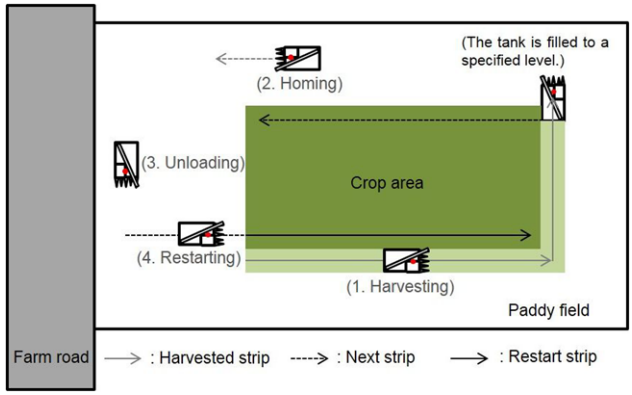

Figure 3. Plan for the robotic harvesting operation. The wagon does not appear in this figure; the robot does not know the wagon's position beforehand.

limited the positioning of the combine robot and the wagon. Under this system, the robot searched for a fiducial marker on the wagon roof by rotating its unloading auger with a fixed camera (Figure 2). To enable efficient searching for the marker, Kurita et al. (2014) computed the camera's field of view and developed a marker searching method. At the same time, the difficulties and limitations of this method were analyzed based on numerical simulations (Kurita, 2013). Simulation results indicated that it would become more difficult for the auger camera system to detect the wagon as the height of the farm road increased, and that the location of the wagon would therefore be substantially constrained by that of the robot.

The latter conclusion especially is a critical constraint for practical field operations. In the auger camera system, two points were defined: the unloading position for the robot and the waiting point for the wagon, which had to be located within a specific area dictated by the unloading position. Although the system worked well if the wagon was parked within this area, it failed to detect the marker if the wagon was outside it. Moreover, these two points were fixed throughout the harvesting of a field. The auger camera system therefore worked on the assumption that the wagon would always be located at or very close to a predetermined position on the road. Unfortunately this is impractical, because the wagon is driven by a human driver and he/she has to shuttle between the field and the drying facility several times during the harvesting process. This system is therefore not applicable to actual operations.

3. AUTONOMOUS OPERATION FRAMEWORK

In this section, we present an operation framework for practical autonomous harvesting. In human operation framework, a pair of farmworkers, the operator of a combine, and the driver of a wagon, cooperate for rice harvesting. As described in Section 2.2, the previously developed robot partially automatized rice harvesting and therefore still remains an operator-assisted system as a whole. An autonomous operation framework, on the other hand, would enable harvesting without a human operator and would be designed to work in conjunction with the wagon driver.

In this framework, an integrated algorithm is required for the entire robotic operation. The requirements of the system include that harvesting must be performed with sufficient precision and without leaving any unharvested crops. For unloading, the auger spout must be positioned over the wagon with sufficient accuracy, and more importantly, the algorithm must be able to deal with varying wagon positions in order to work in conjunction with the wagon driver. The framework therefore just assumes that the wagon is located somewhere on the road. In addition, the robot needs to be able to move itself from the harvesting location to the wagon ("homing") and then back to the harvesting ("restarting") (Figure 3).

The complete robotic operation is outlined in Figure 4. First, the combine robot plans the target path and begins the harvesting operation. When the grain tank is filled with grain to a specified level, the combine robot returns to the farm road. The robot then locates the wagon and unloads the grain. If unharvested crop remains, the robot replans the target path and restarts the harvesting operation. Thus, the robotic operation consists of four tasks: harvesting, homing, unloading, and restarting.

When the robotic operation is conducted according to the integrated algorithm (Figure 4), no operator is required for robot maneuvering. The wagon driver has only to wait for the grain to be unloaded into the wagon, and to collect the grain from all the fields. In this framework, the combine must still be driven manually between fields, but this is not a frequent operation and requires far fewer operators than the number of combine robots in use.

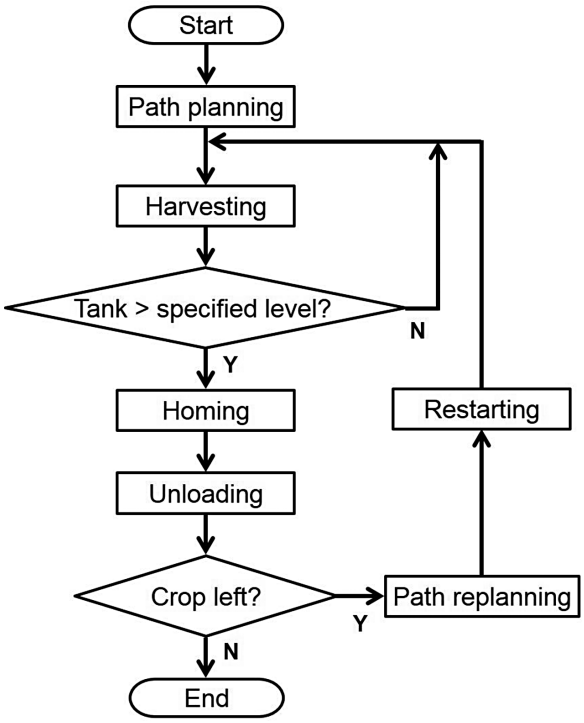

Figure 4. Principal flow of the integrated algorithm for fully automated robotic rice harvesting.

Overall, this framework requires fewer farmworkers than the conventional manual operation framework, and tasks that require skill and concentration can be delegated to robots.

3.1. Harvesting

This section details each part of the integrated algorithm. The path-following control is based on the method of Iida et al. (2013). Here, we consider briefly the path planning and turning processes.

The header and cutting device of a head-feeding combine is fixed and aligned along the left side of the combine body. Hence, the combine is best suited to harvest crops along a counterclockwise path such that the header is aligned with the crop rows. The path pattern on a rectangular field results in a counterclockwise spiral path (called a "round-harvesting path" in this study). The robot plans its round-harvesting path before it commences operation, and then follows it. The path consists of two simple operations: straight travel and right-angle turns to the left. In a Japanese rice paddy, rice plants are typically planted in rows with 0.3 m spacing. If the rice is harvested using the maximum swath width, a combine harvester sometimes divides a crop row, which should be avoided because it often results in unharvested rice being left behind. In addition, the VY50 robot can deviated from the target path by $\pm$ 0.1 m, so the current robot should also take into account a margin of error when planning its path to prevent unharvested crops remaining. This margin is set to 0.3 m. Hence, the combine robot tolerates a lateral error in its target path of up to $\pm$ 0.15 m. The robotized combine harvester used in this study is a four-row head-feeding model, which reaps four rows even with this tolerated overlap.

When the robot reaches the end of a strip, it has to turn left and align its heading with the next strip. The combine can turn in place without going forward or backward by driving the tracks counter-directionally (pivot turning), yet this causes severe damage to the ground, especially as rice paddy fields are relatively muddy in comparison to those of other crops. As pivot turning should therefore be avoided, the combine robot performs its left turn with a less efficient but also less damaging method called "switchback turning". The robot therefore switchbacks at the end of the current strip to enter into the next strip.

3.2. Homing

The combine robot checks the capacity of its grain tank at the end of each harvested strip. If the tank is filled to the specified, the robot transitions to the homing operation. A homing path is generated from the end of the current strip to a line parallel to the farm road ("baseline"). Depending on the point at which the tank reaches the specified level, the homing path can take one of four patterns (Figure 5).

In patterns 1 and 2, to ensure that the robot does not run over the unharvested area, Points A_0 and A_1 are placed so as to be at least L_{margin} from the crop area (in this study L_{margin} is set to 2.5 m; Figure 5). Point B is the intersection of the baseline and the perpendicular line to the baseline from Point A_1. In pattern 3, Point A_1 is identified as the end of the current strip. The robot creates the homing path by proceeding from Point A_0 (pattern 1 only) to Point A_1 to Point B, with the exception of pattern 4. The line CD is the baseline. Its length and location can be decided arbitrarily, although it needs to be sufficiently close to the farm road to allow the robot to unload the rice into a wagon parked on the road. This proximity makes it difficult and sometimes impossible for the robot to follow the homing path in the final approach to the baseline, because the robot may crash into the farm road, as illustrated in patterns 2 and 4 (Figure 5). To avoid this, the robot follows a specific procedure in the final approach.

Figure 6 represents the final approach for patterns 1, 2, and 3 (left) and 4 (right). For patterns 1, 2, and 3, the robot turns left by angle γ_1 at Point E (distance D_1 before it reaches Point B), and goes straight until it reaches the baseline. It then turns left by the remaining angle required to make a right angle, that is, $90° - \gamma_1$. In pattern 4, the robot returns by traveling in reverse. At the end of the strip, it turns left

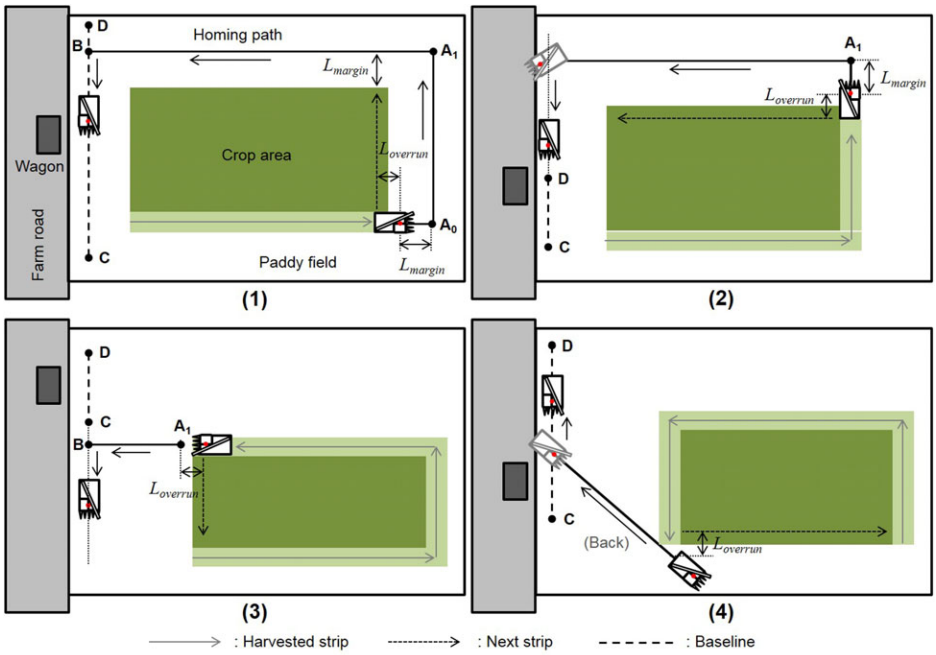

Figure 5. The four patterns of possible homing path taken by the robot depending on its location when the grain tank reaches the specified filling level. The homing path is planned so as to allow sufficient distance from the unharvested area to ensure that no unharvested crops are run over. The line CD indicates the baseline. Its length and location can be defined arbitrarily, as indicated by the variation in these diagrams. The robot returns to the baseline by traveling forward in patterns 1, 2, and 3, but by traveling backward in pattern 4. Patterns 2 and 4 show the robot (gray) entering the farm road, which must be avoided.

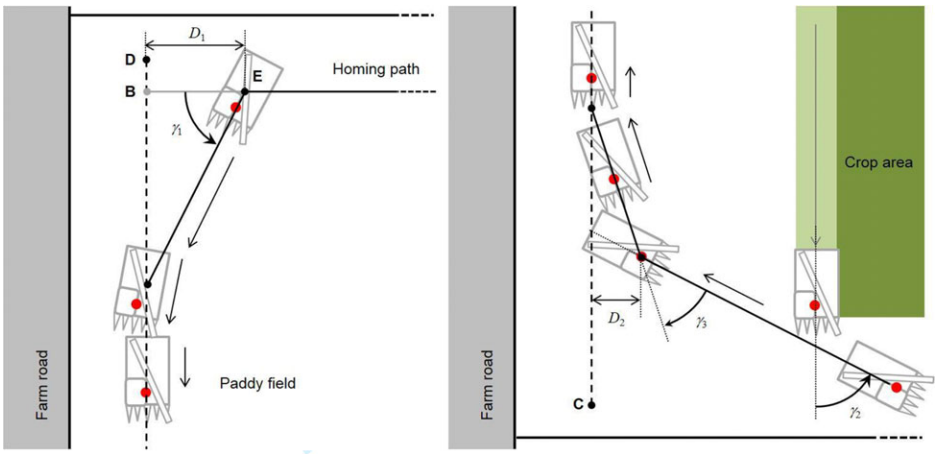

Figure 6. The turning method used by the robot in the final approach to the baseline. Left: the robot turns left before reaching Point B in homing patterns 1, 2, and 3. It travels forward until reaches the baseline and then aligns itself with the baseline. Right: when following homing pattern 4, the robot first turns left at the end of the current strip. It travels backward and then turns right in two steps to align itself with the baseline.

by acute angle γ_2 and travels straight backward. When the distance between the robot and the baseline is D_2, the robot turns right by a smaller acute angle γ_3 and continues to travel until it reaches the baseline. Finally, it turns right by the remaining angle, $\gamma_2 - \gamma_3$, to align its heading to the baseline.

At the end of the homing operation, the remaining crop area is recorded. The robot runs at 0.8 m/s during the

homing operation, except in the final approach (0.5 m/s), and slows to 0.3 m/s at corners. By using this approach method, the robot can smoothly change lanes without collision with the farm road, which ensures that the unloading can proceed successfully.

3.3. Unloading

3.3.1. Machine Vision System

In order to automate the unloading operation, the combine robot is required to recognize the wagon and position its auger spout at an appropriate point over the wagon. As described in Section 2.2, a machine vision system was developed by Kurita, Iida, and Suguri (2012) that consisted of a camera on the unloading auger and a planar fiducial marker on the wagon roof. However, the system had serious drawbacks for application to an uninterrupted harvesting and unloading operation. We have developed an improved method in this study. We used the same marker as used by Kurita et al. (2012), and the robot's control program uses the ARToolKit library (Kato & Billinghurst, 1999) to detect the fiducial marker and estimate camera pose relative to the marker. However, in our system the camera is mounted on the top of the grain tank, facing the backward of the combine. Therefore, the fiducial marker is attached to one side of the wagon. Figure 7 shows the camera and the wagon with the marker.

Figure 7. Machine vision system. Top left: a camera is mounted on the top of the grain tank. Top right: a fiducial marker is fixed to one side of the wagon. Bottom: the machine vision system in operation in a paddy field. The wagon is parked on the farm road, the height of which above the field varies among fields. The captured image is processed by the robot's control computer (not shown).

3.3.2. Kinematics of the Unloading Auger

The unloading auger of the combine can be modeled as a 2-degree-of-freedom (DOF) mobile manipulator. As shown in Figure 8, a Cartesian coordinate system Σ_0 is assigned to the combine. In this study, we use a right-handed Cartesian system. Two joint angles are denoted by θ_1 and θ_2.

The link structure of the unloading auger is shown in Figure 9. Σ_{Marker} and Σ_{Camera} are marker-based and camera-based coordinate systems, respectively.

In Σ_0, the position of the auger spout, ${}^0\boldsymbol{r}_{\text{Spout}}$, is described according to direct kinematics. In order to represent the spout position, two coordinate systems Σ_1 and Σ_2 are attached to Joint 1 and Joint 2, respectively. Σ_1 represents the rotation θ_1 of Joint 1 with respect to Σ_0. Σ_2 is obtained by rotating Σ_1 around the Y_1 axis by angle $-\theta_2$ and translating it by l_a in the Y_1 direction. The transformation from Σ_1 to Σ_0 and Σ_2 to Σ_1 are specifically described as follows:

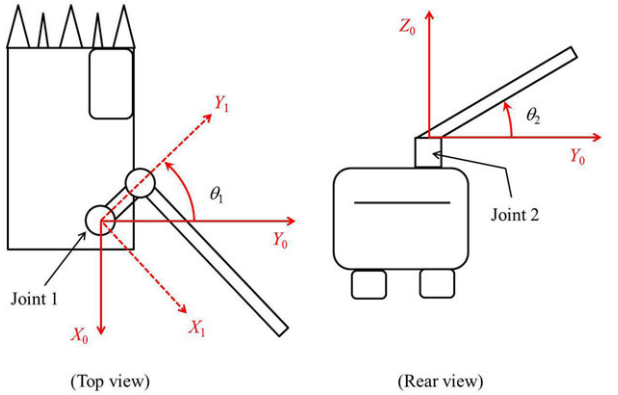

Figure 8. A 2-DOF manipulator model. Joint 1 rotates the unloading auger around the Z_0 axis, transforming the O_0-$X_0Y_0Z_0$ frame, which is fixed with respect to the vehicle body, to an O_1-$X_1Y_1Z_1$ frame (top view). Joint 2 moves the unloading auger upward or downward (rear view).

$$ {}^0T_1 = \begin{bmatrix} \cos\theta_1 & -\sin\theta_1 & 0 & 0 \\ \sin\theta_1 & \cos\theta_1 & 0 & 0 \\ 0 & 0 & 1 & 0 \\ 0 & 0 & 0 & 1 \end{bmatrix} \tag{1} $$

$$ {}^1T_2 = \begin{bmatrix} \cos\theta_2 & 0 & -\sin\theta_2 & 0 \\ 0 & 1 & 0 & l_a \\ \sin\theta_2 & 0 & \cos\theta_2 & 0 \\ 0 & 0 & 0 & 1 \end{bmatrix}, \tag{2} $$

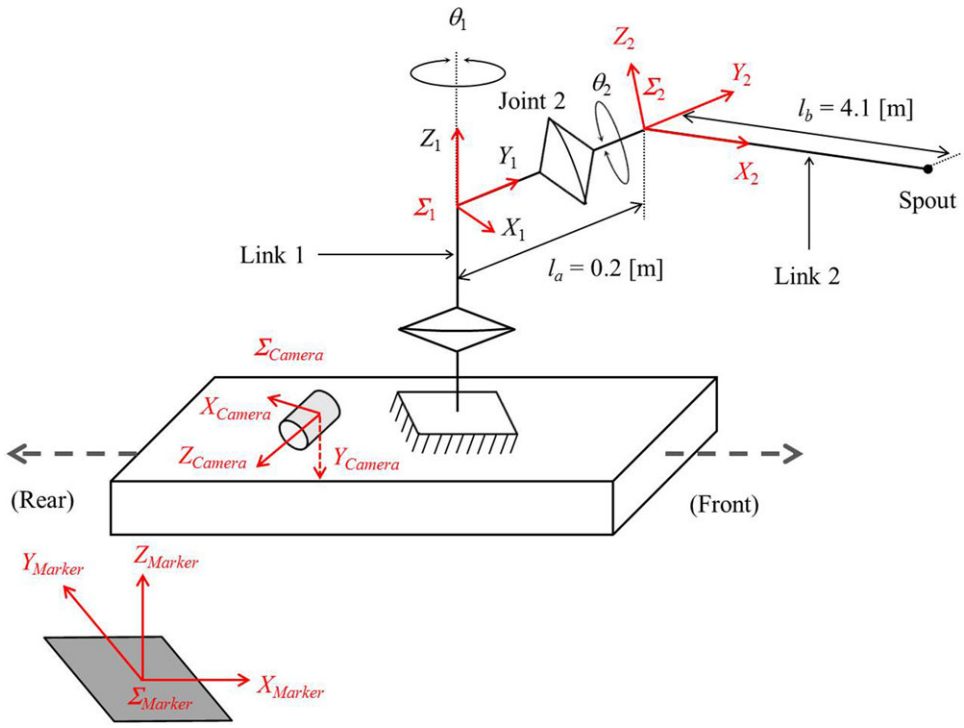

Figure 9. Link structure of the mobile manipulator.

where ${}^{N}\boldsymbol{T}_{M}$ is the homogeneous transformation matrix from Σ_M to Σ_N. ${}^{2}\boldsymbol{r}_{\text{Spout}}$, the spout position in Σ_2, is given by $[l_b, 0, 0, 1]^T$. ${}^{0}\boldsymbol{r}_{\text{Spout}}$ is thus obtained as

$$
\begin{aligned}
{}^{0}r_{\text{Spout}} &= {}^{0}T_1\,{}^{1}T_2\,{}^{2}r_{\text{Spout}} \\
&= \begin{bmatrix} l_b\cos\theta_1\cos\theta_2 - l_a\sin\theta_1 \\ l_b\sin\theta_1\cos\theta_2 + l_a\sin\theta_1 \\ l_b\sin\theta_2 \\ 1 \end{bmatrix}.
\end{aligned} \tag{3}
$$

If ${}^{\text{Marker}}\boldsymbol{r}_{\text{Target}}$ denotes the position of the target point in Σ_{Marker}, then the same point is represented in Σ_0 as

$$
{}^{0}r_{\text{Target}} = {}^{0}T_{\text{Marker}}\,{}^{\text{Marker}}r_{\text{Target}}. \tag{4}
$$

${}^{0}\boldsymbol{T}_{\text{Marker}}$ can be decomposed as

$$
{}^{0}T_{\text{Marker}} = {}^{0}T_{\text{Camera}}\,{}^{\text{Camera}}T_{\text{Marker}}, \tag{5}
$$

where ${}^{0}\boldsymbol{T}_{\text{Camera}}$ is constant and can be measured offline. As shown in Figure 10, Σ_0 is transformed into Σ_{Camera} by the translation of $-l_c$, l_d, and $-l_e$ in the X_0, Y_0, and Z_0 directions, respectively, and by rotating by angle $-\alpha$ around the Z_0 axis and $-\beta$ around the X_{Camera}' axis (l_c, l_d, l_e, α, $\beta \geq 0$). Hence, we have

$$
{}^{0}T_{\text{Camera}} = \begin{bmatrix} \cos\alpha & \sin\alpha\cos\beta & \sin\alpha\sin\beta & -l_c \\ -\sin\alpha & \cos\alpha\cos\beta & \cos\alpha\sin\beta & l_d \\ 0 & -\sin\beta & \cos\beta & -l_e \\ 0 & 0 & 0 & 1 \end{bmatrix}. \tag{6}
$$

${}^{\text{Camera}}\boldsymbol{T}_{\text{Marker}}$ represents the camera pose relative to the fiducial marker (i.e., the wagon), which is estimated online using the machine vision system, as described in Section 3.3.1. Let p_{ij} be the (i, j) entry in matrix ${}^{\text{Camera}}\boldsymbol{T}_{\text{Marker}}$. The target point of the spout with respect to the marker, ${}^{\text{Marker}}\boldsymbol{r}_{\text{Target}} = [t_x, t_y, t_z, 1]^T$, is a constant value. Then the target position in Σ_0 is obtained from Eqs. (4) and (5) as follows:

$$
\begin{aligned}
{}^{0}r_{\text{Target}} &= {}^{0}T_{\text{Camera}}\,{}^{\text{Camera}}T_{\text{Marker}}\,{}^{\text{Marker}}r_{\text{Target}} \\
&= \begin{bmatrix} \cos\alpha & \sin\alpha\cos\beta & \sin\alpha\sin\beta & -l_c \\ -\sin\alpha & \cos\alpha\cos\beta & \cos\alpha\sin\beta & l_d \\ 0 & -\sin\beta & \cos\beta & -l_e \\ 0 & 0 & 0 & 1 \end{bmatrix} \begin{bmatrix} p_{11} & p_{12} & p_{13} & p_{14} \\ p_{21} & p_{22} & p_{23} & p_{24} \\ p_{31} & p_{32} & p_{33} & p_{34} \\ 0 & 0 & 0 & 1 \end{bmatrix} \begin{bmatrix} t_x \\ t_y \\ t_z \\ 1 \end{bmatrix}.
\end{aligned} \tag{7}
$$

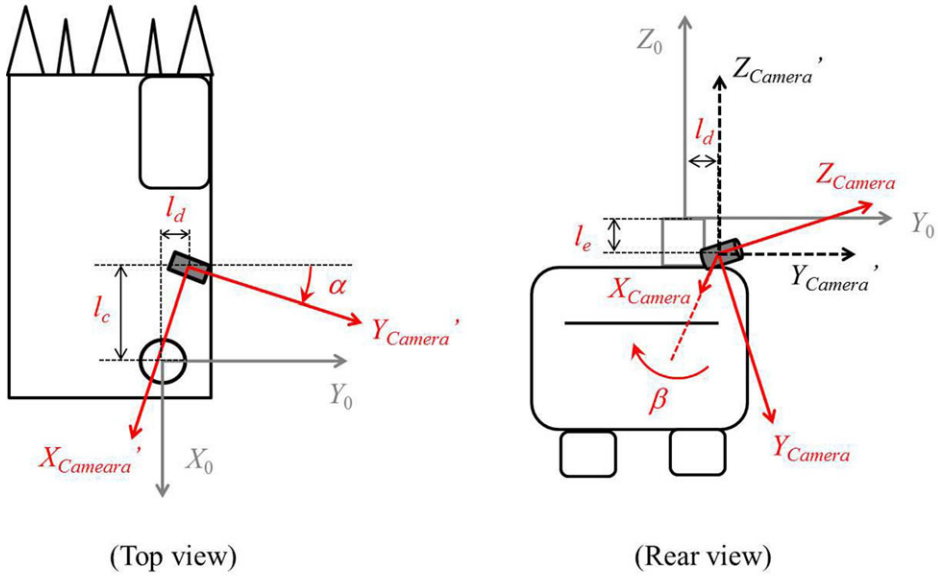

Figure 10. Camera frame configuration. The camera-based coordinate system is offset from Σ_0 by l_c, l_d (top view), and l_e (rear view). Top view: Σ_0 is rotated around the Z_0 axis into the O_{Camera}'-$X_{\text{Camera}}'Y_{\text{Camera}}'Z_{\text{Camera}}'$ frame. Rear view: O_{Camera}'-$X_{\text{Camera}}'Y_{\text{Camera}}'Z_{\text{Camera}}'$ frame is rotated around the X_{Camera}' axis into the camera-based frame O_{Camera}-$X_{\text{Camera}}Y_{\text{Camera}}Z_{\text{Camera}}$. The X_{Camera}' axis is not shown but identical to the X_{Camera} axis.

Finally, the target joint angles θ_1 and θ_2 are determined such that they satisfy

$$ {}^0r_{\text{Spout}} = {}^0r_{\text{Target}}. \tag{8} $$

If we abbreviate the result of Eq. (7) as $[T_x, T_y, T_z, 1]^T$, Eqs. (3) and (8) give

$$ l_b \cos\theta_1 \cos\theta_2 - l_a \sin\theta_1 = T_x \tag{9} $$

$$ l_b \sin\theta_1 \cos\theta_2 + l_a \cos\theta_2 = T_y \tag{10} $$

$$ l_b \sin\theta_2 = T_2. \tag{11} $$

In most cases, θ_1 and θ_2 cannot satisfy Eq. (8) simultaneously for all three coordinates, since the unloading auger itself only has 2 DOF. To fulfill Eq. (8) in three dimensions, traveling on part of the combine robot is required (Kurita et al., 2012). The vision system calculates a provisional solution of Eqs. (8), (9), and (10).

$$ \begin{cases} \theta_{1\_\text{prov}} = \cos^{-1}\left(\dfrac{l_a}{\sqrt{T_x^2 + T_y^2}}\right) - \tan^{-1}\left(\dfrac{T_x}{T_y}\right) \\ \theta_{2\_\text{prov}} = \cos^{-1}\left(\dfrac{\sqrt{T_x^2 + T_y^2 - l_a^2}}{l_b}\right). \end{cases} \tag{12} $$

Then, Z_{Error}, the positioning error in the Z_0 direction, can be estimated using Eq. (11).

$$ Z_{\text{Error}} = T_z - l_b \sin\theta_{2\_\text{prov}}. \tag{13} $$

In practice, the vision system determines a pair of angles $(\theta_{1\_\text{prov}}, \theta_{2\_\text{prov}})$ as a numerical solution of Eq. (8) that satisfies Eq. (14).

$$ \| Z_{\text{Error}} \| \leq \varepsilon, \tag{14} $$

where $||\cdot||$ denotes the Euclidean norm. ε defines the tolerance in the Z_0 direction, and it was set to 0.3 m in this study. The robot is therefore required to identify the vehicle position at which θ_{1_prov} and θ_{2_prov} fulfill Eq. (14).

The auger camera system is designed to work when the two vehicles are arranged in specific positions. Although the robot may be able to position itself with a high degree of accuracy, it is unlikely that a human driver would be able to precisely park the wagon at a specific waiting point at all times when shuttling repeatedly between the field and the drying facility.

A simple solution is to move the vehicle on a line parallel to the farm road (the baseline in Section 3.2). Since the wagon will be parked somewhere on the farm road, the robot is expected to recognize the wagon while moving parallel to the road. The machine vision system was thus developed as shown in Figure 7. As the vehicle moves along the baseline, the vision system will capture the marker. In addition, there must exist at least one point on the line

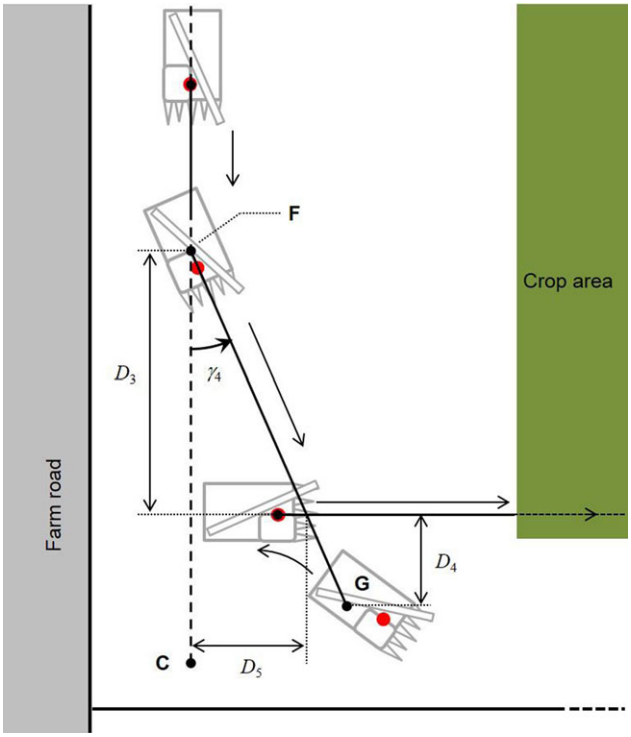

Figure 11. The restarting operation performed by the robot upon completion of unloading. The robot travels along the baseline to Point F. It travels backward if the point is behind the unloading position, or forward if it is in front. The diagram shows the latter case.

at which Eq. (14) is met. The combine robot searches for the wagon from the baseline, first traveling forward to one end of the baseline (Point C) and then backward to the other end (Point D). Using the homing algorithm, the robot returns to the baseline, or more precisely to an extension of the baseline. Sometimes the robot is not on the baseline when the homing operation is completed. Patterns 2 and 3 of Figure 5 illustrate this case. In the case shown in pattern 2, the unloading operation is performed as described above (to Point C and then to Point D). In that the case shown in pattern 3, the forward traveling is skipped, and the robot only moves backward to Point D.

In this study, the searching operation is performed at 0.5 m/s. The robot slows to 0.2 m/s when the wagon is detected, and immediately stops if Eq. (14) is satisfied. The grain is discharged after the spout is positioned successfully.

3.4. Restarting

Upon completion of the unloading operation, the combine robot replans the target path on-board based on the remaining crop area, then moves to an extension of the first strip in the new target path (Figure 11). To perform this transfer, the robot first travels along the baseline to Point F. This point is determined so as to be distance D_3 away from the first strip. From Point F, the robot turns left by angle γ_4 and goes straight, past the first strip by distance D_4, to Point G. On reaching Point G, the robot performs switchback turning and aligns its heading before restarting the harvesting operation.

The robot leaves the baseline in a similar manner to that used in the final approach during the homing operation (Figure 6). This is because the robot cannot usually perform a large-angle turn on or close to the baseline. The distance from Point G to the baseline, D_5, has to allow sufficient space for switchback turning, so D_3 is calculated based on D_5 and γ_4.

The restart strip is selected as the nearest longitudinal strip from the original first strip in order to apply the round-harvesting technique to the continuous harvesting operation. If there is no remaining crop to harvest, the combine robot stands by at the unloading position. The restarting operation stated above is also done autonomously by the robot.

4. FIELD TEST

4.1. Experimental Condition

We conducted field tests in actual paddies in order to evaluate the control algorithms and the performance of our combine robot. The tests were carried out in rice paddies in Nantan City, Kyoto, Japan, on October 14, 2013 (Test 1), and in Tsukuba City, Ibaraki, Japan, on September 16 (Test 2) and 17 (Test 3), 2014. The fields were approximately rectangular, with dimensions of 92.15 m × 28.25 m (Test 1), 98.91 m × 35.67 m (Test 2), and 96.30 m × 30.65 m (Test 3). The weather was clear and sunny during all tests. We manually harvested the outer area of the fields for several laps before beginning the automated harvesting. This was done for two reasons: first, switchback turning requires a much larger area than pivot turning, and there must be sufficient space between the unharvested crop area and the embankments around the fields; second, the combine may deviate from the target path for unexpected reasons during the tests. If this occurs near the embankment, the combine may touch or run into it, which can cause significant mechanical damage. It was therefore decided to keep a reasonable safety distance from the embankments.

The combine was manually deployed at a point on an extension of the first strip. The distance from this point to the edge of the crop area was measured and input into the control program. The harvesting speed was set to 0.6 m/s (Test 1), 0.8 m/s (Test 2), and 1.0 m/s (Test 3) to analyze its effect on the total required time. In addition, the control program required the following information: the dimension of the crop area (78.0 m × 11.7 m in Test 1, 88.8 m × 27.3 m in Test 2, and 81.2 m × 23.0 m in Test 3), the orientation of the first strip, the absolute position of the starting point, the

Figure 12. Combine robot and sensors.

Table I. Specifications of the base machine.

Model	VY446LM
Dimension, mm	
Length	4,010
Width	1,900
Height	2,700
Weight, kg	2,380
Engine	S4L2–T13C
Type	4–cycle, water-cooled diesel
Output, kW (PS)/rpm	33.8 (46) / 2,800
Grain tank, L	1,050

length of the baseline (10.0 m in Test 1 and 6.0 m in Tests 2 and 3), and the duration of discharging; the combine robot discharges the grain just for this duration after the spout is positioned. This was set to 90 s in this study based on experimental findings.

4.2. Mechanical Configuration

Figure 12 shows the combine robot developed in this study. The base machine is a four-row head-feeding combine harvester VY446LM (Mitsubishi Agricultural Machinery, Shimane, Japan), a crawler type vehicle. Table I summarizes the specifications of the base machine. Three volume levels of harvested grain can be approximately specified: 400 L, 600 L, and 1,050 L. Upon reaching the third level, the engine will stop automatically for safety reasons.

A multiglobal navigation satellite system (Multi-GNSS, referred to as GNSS hereafter) receiver AGI-3 (Topcon, Tokyo, Japan) is used to locate the vehicle position. This is able to handle both Global Positioning System (GPS) and Globalnaya Navigatsionnaya Sputnikovaya Sistema (GLONASS) signals. AGI-3 supports real-time kinematic surveying, for which a virtual reference station system is adopted. A personal digital assistant iPAQ hx2190b (Hewlett-Packard, Palo Alto, CA) and mobile Wi-Fi router L03E (Docomo, Tokyo, Japan) are used in reference stations. In addition, vehicle orientation is measured with a GPS compass ssV-102 (Hemisphere, Scottsdale, AZ). Both sensors are attached to the cab roof (Figure 12). The GNSS antenna is located on the center divider of the cutting device's header. Measured absolute position and orientation, with an accuracy of $\pm$ 30.0 mm and $\pm$ 0.50°, respectively, is utilized for vehicle navigation. A camera UCAM-DLA200H (Elecom, Osaka, Japan) is mounted on the top of the grain tank, with a 1/4 inch CMOS image sensor, a focal length of 4.3 mm, and a diagonal angle of view of 60°.

5. RESULTS AND DISCUSSION

The original target path and the recorded path of the combine robot in Test 1 are shown in Figure 13. The horizontal axis corresponds to the direction of the first strip. The center of the baseline is set as the origin. The robot performed the unloading operation twice in this experiment. The operation from the departure until the end of the first unloading will hereafter be referred to as Cycle 1 and that from the end of the first unloading until the end of the whole operation as Cycle 2.

Tracking performance on the straight path in Test 1 is summarized in Table II. The root mean square error (RMSE) of the lateral error from the target path was less than 0.04 m, and the RMSE of the azimuth error from the target direction was less than 2.6°. The lateral error and the azimuth error were no less than 0.08 m and 4.5°, respectively, with the exception of strip 2–3 (0.12 m and 8.4°), where errors were increased since they were recorded in the approaching phase soon after turning and before the next harvesting. In this phase, the combine robot adjusts its position and orientation to an extension of the next strip.

Figure 14 shows variation of lateral and azimuth errors in strip 2–3. The horizontal axis indicates the travel distance immediately after the completion of the turning stage. Large errors appeared at the beginning of travel, which was probably caused by the soil conditions; the ground was so muddy that the crawler foot sank to half its height in the mud, but corrected immediately. Lateral error decreased to less than 0.05 m in 1.60 m of travel, while azimuth error became $-2.0°$ in 2.20 m of travel. Subsequently both errors fell to approximately within $\pm$ 0.05 m and $\pm$ 2.0°, respectively. In this experiment, the control program assigned 1.4 m of travel to the approaching phase. Although these errors are quite large, they became tolerable when the robot actually reached the crop area. Taken together, all crop was successfully harvested, including strip 2–3.

Figures 15 and 16 show the vehicle trajectories in Tests 2 and 3, respectively, but the trajectory during the unloading operation is excluded here. Each of the homing patterns was tested: pattern 1 in Cycle 1 of Test 1 and Cycle 1 of Test 3; pattern 2 in Cycle 2 of Test 2; pattern 4 in

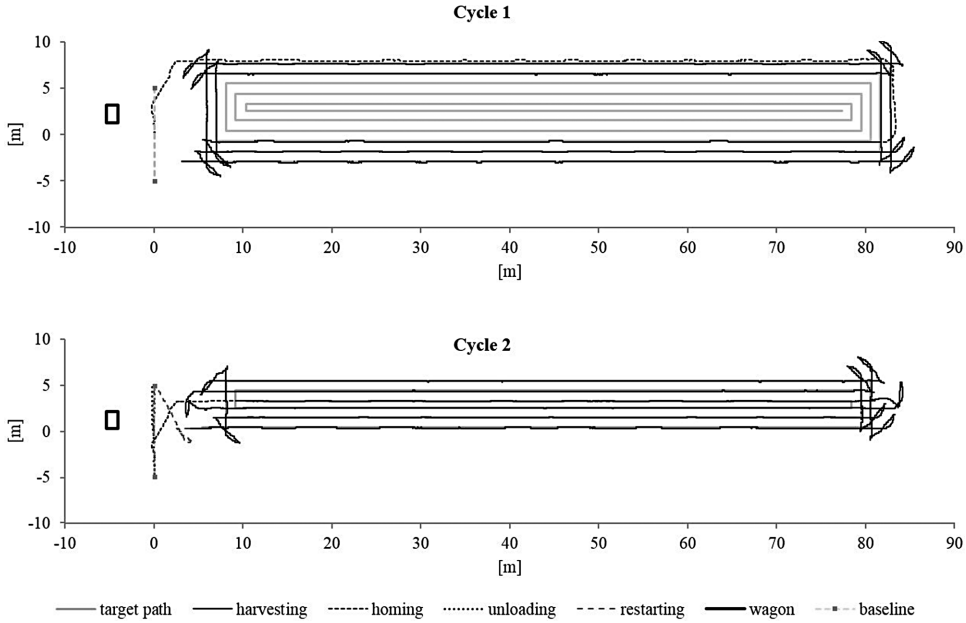

Figure 13. The target path and trajectory of the robot in Test 1.

Table II. Tracking performance on the straight path in Test 1.

	Lateral error [m]					Azimuth error [°]				
Strip No.	Max	Min	Mean	RMSE	STD	Max	Min	Mean	RMSE	STD
1–1	0.08	–0.04	0.02	0.03	0.03	–0.3	–4.3	–2.1	2.3	0.9
1–2	0.05	–0.06	0.01	0.03	0.03	0.5	–2.6	–1.2	1.5	1.0
1–3	0.07	–0.07	–0.01	0.03	0.03	0.1	–4.5	–2.4	2.6	1.0
1–4	0.05	–0.07	0.00	0.03	0.03	1.7	–3.4	–0.4	1.4	1.3
1–5	0.06	–0.04	0.01	0.03	0.03	0.7	–3.8	–1.7	2.0	1.0
1–6	0.05	–0.06	0.00	0.03	0.03	0.7	–2.0	–1.2	1.4	0.8
1–7	0.06	–0.07	–0.01	0.03	0.03	1.6	–3.6	–1.4	1.8	1.0
1–8	0.05	–0.07	0.00	0.03	0.03	1.0	–3.8	–0.4	1.3	1.2
1–9	0.06	–0.08	–0.01	0.03	0.02	1.4	–3.8	–0.7	1.1	0.9
2–1	0.07	–0.05	0.01	0.03	0.03	1.2	–3.4	–1.4	1.7	1.0
2–2	0.05	–0.07	–0.01	0.04	0.04	–0.1	–3.8	–1.7	2.1	1.1
2–3	0.10	–0.12	0.01	0.03	0.03	1.0	–8.4	–1.0	1.6	1.3
2–4	0.06	–0.07	0.01	0.04	0.04	0.9	–2.3	–0.7	1.2	1.0
2–5	0.08	–0.06	0.01	0.03	0.03	1.5	–2.7	–0.8	1.2	0.9
2–6	0.07	–0.06	–0.01	0.04	0.04	0.5	–1.8	–0.2	0.7	0.7
2–7	0.06	–0.07	–0.01	0.03	0.03	1.3	–3.6	–1.0	1.4	0.9
2–8	0.08	–0.07	0.00	0.03	0.03	1.3	–4.5	–0.8	1.3	1.0
2–9	0.06	–0.06	0.00	0.03	0.03	2.1	–2.4	–0.4	1.1	1.0

Cycle 3 of Test 2; and pattern 3 in the remaining cycles. Table III lists the lateral error and the azimuth error from the baseline on completion of the homing operation. The RMSE of the lateral and azimuth errors was 0.07 m and 3.6°, respectively; error magnitude in most cases was no greater than 0.1 m and 4°, respectively. This indicates that the robot transferred itself sufficiently close to the baseline and aligned its heading almost parallel to the farm road, as planned.

After returning to the baseline, the unloading operation was performed. Positioning accuracy of the auger spout is shown in Table IV. Positions are represented in coordinate

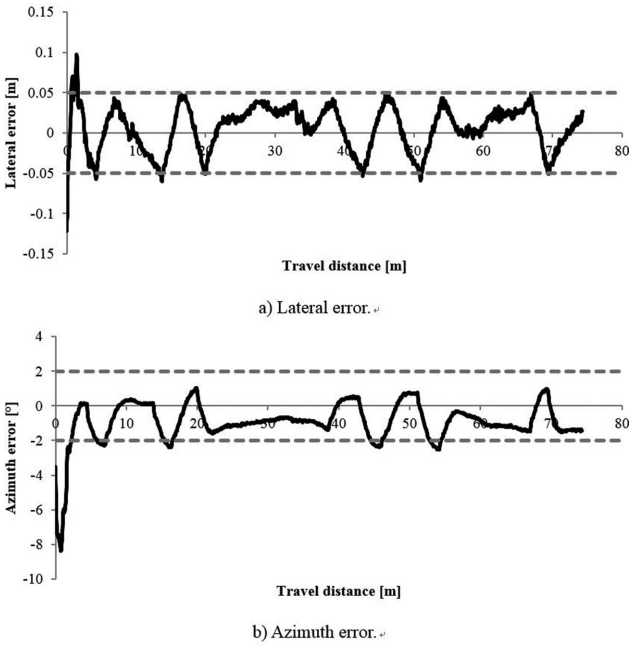

Figure 14. The lateral and azimuth errors in strip 2–3. Large errors appeared only at the beginning of the strips 2–3, but had been corrected by the time the robot reached the crop area.

Table III. Lateral and azimuth errors with respect to the baseline on the completion of the homing operation, and the homing pattern of each operation.

		Lateral error [m]	Azimuth error [°]	The homing pattern
Test 1	Cycle 1	–0.12	–3.4	(1)
	Cycle 2	0.02	–3.1	(3)
Test 2	Cycle 1	–0.04	–3.3	(3)
	Cycle 2	–0.10	–4.0	(2)
	Cycle 3	–0.02	4.3	(4)
	Cycle 4	–0.13	–4.2	(3)
Test 3	Cycle 1	0.03	–3.3	(1)
	Cycle 2	–0.04	–4.1	(3)
	Cycle 3	0.05	–1.3	(3)
	Max	0.05	4.3	
	Min	–0.13	–4.2	
	RMSE	0.07	3.6	

system Σ_0. For each cycle, the first row is the target position that was obtained with the machine vision system, ${}^0\boldsymbol{r}_{\text{Target}}$ in Eq. (7). Spout position ${}^0\boldsymbol{r}_{\text{Spout}}$, once the positioning had been performed, is calculated based on the recorded joint angles, and is shown in the second row. Positioning error

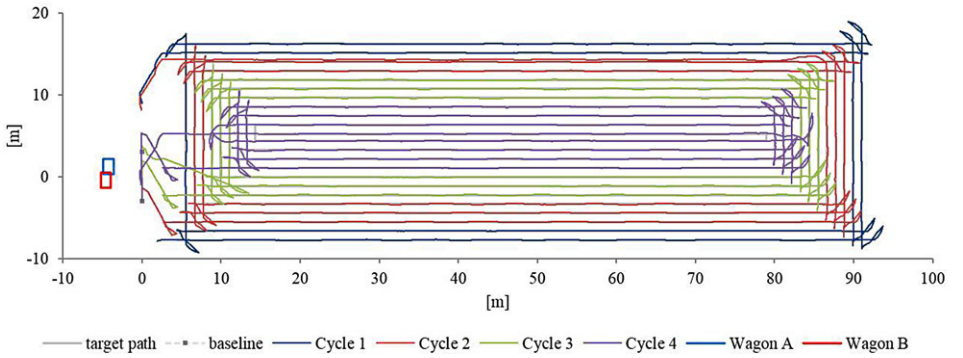

Figure 15. The trajectory of the robot in Test 2. The wagon moved from Wagon A in Cycles 1 and 2 to Wagon B during Cycles 3 and 4.

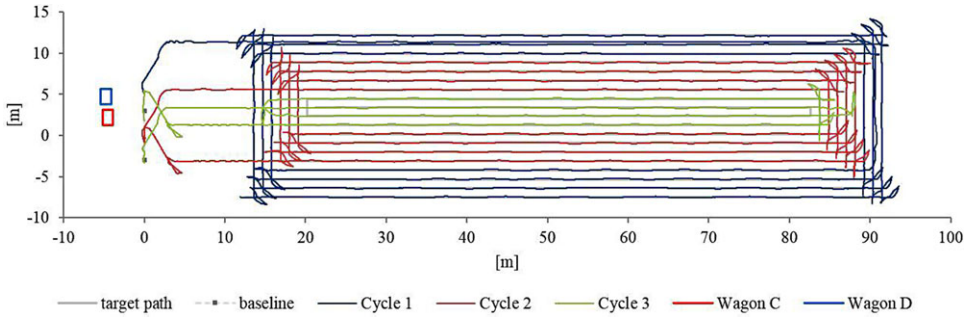

Figure 16. The trajectory of the robot in Test 3. The wagon moved from Wagon C in Cycle 1 to Wagon D during Cycles 2 and 3.

Table IV. Positioning accuracy of the auger spout.

			X_0 [m]	Y_0 [m]	Z_0 [m]
Test 1	Cycle 1	${}^0\boldsymbol{r}_{\text{Target}}$	0.72	4.17	0.69
		${}^0\boldsymbol{r}_{\text{Spout}}$	0.59	3.98	0.81
		Error	–0.13	–0.19	0.12
	Cycle 2	${}^0\boldsymbol{r}_{\text{Target}}$	0.49	4.18	0.72
		${}^0\boldsymbol{r}_{\text{Spout}}$	0.32	4.01	0.81
		Error	–0.17	–0.17	0.09
Test 2	Cycle 1	${}^0\boldsymbol{r}_{\text{Target}}$	1.77	3.44	1.20
		${}^0\boldsymbol{r}_{\text{Spout}}$	1.72	3.48	1.34
		Error	–0.05	0.04	0.14
	Cycle 2	${}^0\boldsymbol{r}_{\text{Target}}$	1.78	3.44	1.15
		${}^0\boldsymbol{r}_{\text{Spout}}$	1.73	3.50	1.28
		Error	–0.06	0.06	0.13
	Cycle 3	${}^0\boldsymbol{r}_{\text{Target}}$	0.50	3.79	1.14
		${}^0\boldsymbol{r}_{\text{Spout}}$	0.35	3.83	1.43
		Error	–0.15	0.04	0.29
	Cycle 4	${}^0\boldsymbol{r}_{\text{Target}}$	0.75	3.78	1.12
		${}^0\boldsymbol{r}_{\text{Spout}}$	0.66	3.81	1.37
		Error	–0.09	0.04	0.25
Test 3	Cycle 1	${}^0\boldsymbol{r}_{\text{Target}}$	1.52	3.92	0.73
		${}^0\boldsymbol{r}_{\text{Spout}}$	1.36	3.79	0.81
		Error	–0.16	–0.13	0.08
	Cycle 2	${}^0\boldsymbol{r}_{\text{Target}}$	1.15	3.89	0.84
		${}^0\boldsymbol{r}_{\text{Spout}}$	1.05	3.88	0.82
		Error	–0.11	–0.01	–0.02
	Cycle 3	${}^0\boldsymbol{r}_{\text{Target}}$	2.12	3.93	0.84
		${}^0\boldsymbol{r}_{\text{Spout}}$	1.96	3.85	0.87
		Error	–0.17	–0.08	0.03

is calculated as ${}^0\boldsymbol{r}_{\text{Spout}} - {}^0\boldsymbol{r}_{\text{Target}}$. In all unloading operations, the auger spout was positioned within $\pm$ 0.2 m of the target position, in both the X_0 and the Y_0 direction. We set $\pm$ 0.2 m as an acceptable tolerance for positioning, as reported in Kurita et al. (2012). This range is appropriate for preventing grain spillage, based on the typical size of the container (1.83 m $\times$ 1.3 m $\times$ 1.17 m) mounted on a truck deck that is widely used as a wagon by Japanese farmers.

There were some general tendencies in the error values. In Test 2, the error on the X_0 axis tended to be negative, while that on the Y_0 axis tended to be positive, but in Tests 1 and 3 the error was negative on both axes. Both the distance between the baseline and the wagon, and the height of the farm road above the field, were roughly constant in each field but differed between fields. Accordingly, the relative positions of the robot and the wagon were similar in each field when the spout positioning was carried out. In addition, the auger positioning is probably uniformly affected by the pose estimation and other error sources that are not taken into account in our method, such as the modeling error between a pinhole camera model and the camera used, and between the link structure model and the unloading auger used. A slightly larger error in the Z_0 direction can be tolerated, because the grain flows almost vertically down from the auger spout. The error on the Z_0 axis was generally positive in value. This is because the baseline must be close enough to the farm road that the auger spout will reach over the wagon; thus when the vision system first recognizes the marker, the error decreases until it falls within the acceptable range in the Z_0 direction. This is defined by ε in Eq. (14) and was set to 0.3 m in this study. The results meet the required accuracy; in fact the combine robot discharged the grain into the wagon without any spillage. The size of the wagon used in this study is relatively small compared to those used in other countries; therefore, the autonomous positioning method of this study should be readily applicable to other combine harvesters.

During each test, the driver of the wagon transported the unloaded grain to the drying facility and then returned to the test field. This transportation was performed between Cycles 1 and 2 in Test 1, between Cycles 2 and 3 in Test 2, and between Cycles 1 and 2 in Test 3. Each time, the wagon was located at different positions before and after this operation (Figures 15 and 16). The original auger camera system, as discussed in Section 3.3, could not handle such a scenario. In the tests of the new system, we left the decision about where to park the wagon to the driver. Nevertheless, the robot recognized the wagon and unloaded the grain successfully.

On completion of the unloading operation, the combine robot replanned the target path based on the remaining crop area. Figures 15 and 16 show that the combine robot followed the only path that had not yet been traveled in the previous cycles (this can also be seen in Figure 13). The vehicle trajectories also show that the robot departed slightly from the baseline (Figure 11). Immediately after the combine had aligned the heading to the restart strip, –0.09 m and –9.9° were recorded as the lateral and azimuth errors, respectively, in Test 1. These were reduced to 0.00 m and –0.3° during the approaching phase. Thus, the robot was able to smoothly follow the target path with sufficient precision. As discussed in Section 3.4, the restart strip is the nearest longitudinal strip from the original first strip. This simplifies the operation; the robot can handle the new target path in the same manner as the original one. Hence, the combine can perform the entire operation as consecutive operations from the end of one unloading to the end of the next. This algorithm is generally applicable to rectangular fields.

The robot's slight deviation from the baseline was within acceptable levels, and this part of the operation met the objectives of avoiding contact with the road and avoiding roughening the field surface along the baseline. In both the homing and the restarting operations, the robot deviated slightly from the baseline. The most important part of this operation is avoiding crashing into the farm road, and the robot should also avoid making a large-angle turn on the baseline, to prevent the field surface from being roughened. Since the robot has to repeatedly run along the baseline, it is particularly important to keep the surface

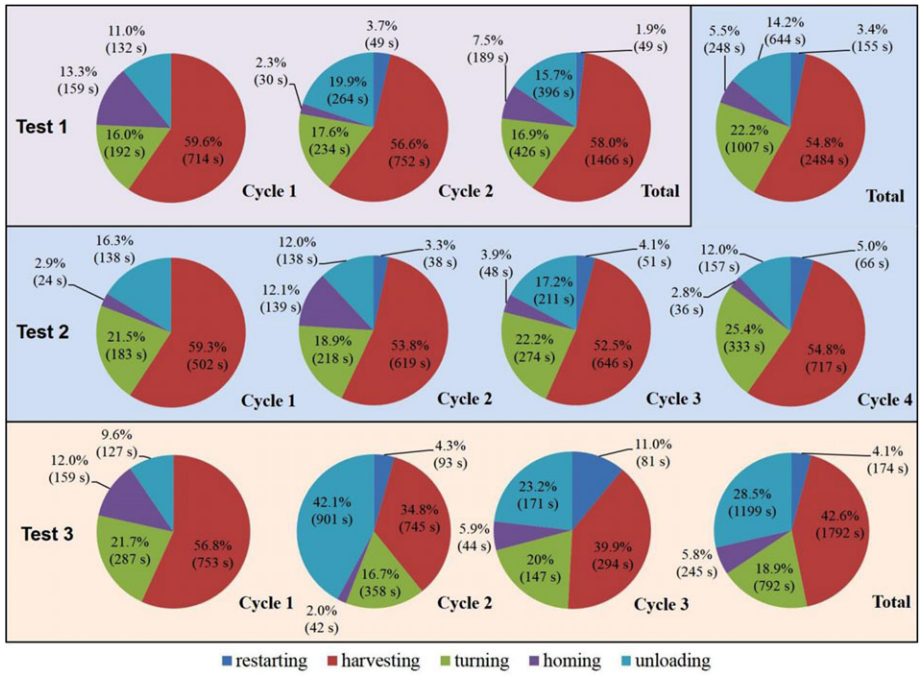

Figure 17. The proportion of time spent on each operation in each test.

smooth for the homing, restarting, and especially unloading operations.

The time taken for each operation is summarized in Figure 17. In Tests 1 and 2, harvesting accounted for approximately 60% and 55% of total working time, respectively. The lower ratio in Test 2 was probably the result of the higher speed (0.8 m/s) used in harvesting. The turning took on average 24 s for one switchback turning process, across all three tests. The homing operation took 3%–6% of the total time, but more than 12% in some cycles, depending on the travel distance to the baseline. The homing operations that followed patterns 1 or 2 (Cycle 1 of Test 1, Cycle 2 of Test 2, and Cycle 1 of Test 3) therefore took longer than the other homing operations. At the present stage of development, the robot decides to perform the homing operation simply based on the grain tank level, which explains these occurrences of inefficient homing. In future development work, the decision to commence the homing operation should be controlled both by the grain tank level and the robot's position, so as to be conducted preferentially using pattern 3 or 4 and thus improve efficiency in terms of time and fuel consumption. This decision making will be more important in the countries with larger fields because of their size and yield.

The unloading operation usually finished within three minutes (including the wagon searching, the spout positioning, and the grain discharging), although it took substantially longer in Cycle 2 of Test 1 (264 s), in Cycle 3 of Test 2 (211 s), and especially in Cycle 2 of Test 3 (901 s). This was because the wagon had not returned from the drying facility when the combine robot had completed the homing operation. Consequently, the combine searched for the wagon but did not find it and reached the terminal of the baseline (Point D in Figure 5). In this scenario, the combine remains at the terminal and waits for instructions from the human operator. In our experiments, we retried the unloading operation after the wagon returned. The time between sending the retry command to the end of unloading was 153 s in Cycle 2 of Test 1, 114 s in Cycle 3 of Test 2, and 106 s in Cycle 2 of Test 3, which is comparable to the other cycles. Harvesting time in Test 3 accounted for approximately 40% of the total, which was notably lower than in the other tests. This was mainly the result of the extended unloading operation discussed above rather than the faster harvesting speed in this test (1.0 m/s). Since the grain discharging duration was given as a constant value (90 s in this study), the rest of the time is mainly consumed traveling along the baseline. The time for the unloading operation can thus be roughly estimated from the discharging duration and the length of the baseline provided as constants to the control program if the wagon is available. The time taken to restart is relatively minimal. The harvesting operation required approximately 50%–60% of the total working time. A simple and effective method to reduce this time is to perform the harvesting operation at higher velocities.

Once a rectangular field dimension is provided and the target path has been created, the total working time of the combine robot can be predicted. The time required for

harvesting can be calculated based upon the harvesting velocity and the total length of the strips. The time for one switchback turn can be regarded as a constant value, since it does not depend on the size of a field but on the turning method. Our experimental results show that the combine requires approximately 24 s per switchback turning, and total turning time can be obtained by multiplying by the number of turns in the target path. A single unload operation requires at least an appropriate discharging duration and the time for locating the wagon. The latter depends on several factors: the length of the baseline, the position of the combine when homing has been completed, and the position of the wagon. These vary depending on the field. It seems reasonable and realistic to empirically define the time for locating it. For the test fields in this study, this was no less than three minutes. In addition, since the combine robot cannot control the wagon's time of return from a drying facility, the combine may search for the wagon despite its absence, as in Cycle 2 of Test 1, Cycle 3 of Test 2, and Cycle 2 of Test 3. This is however an issue with the dispatch control of the wagon rather than the development of the combine robot. The time for the homing operation is presently difficult to predict. The combine needs to schedule the homing operation in the most time- and fuel-efficient way. If an optimal method is established, it is expected that the time for the homing and restarting operations will not exceed 10% of the total working hours.

6. CONCLUSIONS

In this study, we have presented an operation framework for autonomous rice harvesting. The main contribution of the study is to introduce the concept that a robot can perform the entire harvesting operation autonomously. We developed an integrated algorithm for the entire operation, the strength of which is the inclusion of cooperation with farmworkers, which is crucial for practical application of the system in rice paddy fields. Furthermore, we demonstrated its applicability in field experiments using the head-feeding combine robot developed in this study.

In the case of straight path following, the lateral and azimuth errors from the target path and the target direction reached a maximum of 0.12 m and 8.4°, respectively, but in most cases were no larger than 0.08 m and 4.5°. RMSE of the lateral and azimuth errors was 0.04 m and 2.6°, respectively. These results indicate that the combine robot can travel the target path with sufficient accuracy. The larger errors were mainly observed immediately after the completion of the switchback turning process. They were eventually corrected during the approaching phase and became sufficiently small before reaching the next strip. As a result, the robot performed the harvesting by reaping four rows in each strip and without leaving unharvested rice plants.

The combine shifted to the homing operation when the grain tank level reached a predetermined level. It then created the homing path and returned to the baseline without running over the unharvested crop. Performing the unloading operation, the combine robot was able to recognize and locate the wagon using the machine vision system. The unloading auger was modeled as a 2-DOF mobile manipulator. Vehicle position and the two joint angles of the auger were controlled based on the kinematics of the unloading auger and estimated camera pose relative to the wagon. A total of nine unloading operations were executed in our experiment. The auger spout was positioned within $\pm$ 0.2 m of the target point on the horizontal axis and $\pm$ 0.3 m on the vertical axis, which satisfied the requirements of the system. In contrast to the previous system, this combine robot searches for the wagon and identifies the unloading position in one sequence, which solved one of the main limitations of the earlier system. The unloading algorithm presented here is able to handle any uncertainty in the location of the wagon, and in the tests the robot successfully recognized the wagon and discharged the grain even if the wagon's position had changed. After completion of an unloading operation, the robot replanned its target path based on the remaining crop area and traveled to the restart line, aligned its heading to the line, and resumed the harvesting operation. It also made lane changes smoothly and without making large-angle turns on the baseline in both the homing and restarting operations. In summary, the robot harvested the entire crop area and successfully handled variation in conditions introduced by farmworkers.

The harvesting operation required approximately 50%–60% of the robot's total working hours. An increase in speed when it travels along a straight path could improve its efficiency, but this would require a more advanced control for path following. In addition, the homing operation should be scheduled in a more time-efficient manner. On the other hand, the robot had to wait for the wagon several times during the unloading operation. Clearly, the robot's overall efficiency will be diminished in the absence of dispatch control for the wagon. For the efficiency of the harvesting system to be maximized, it would therefore be necessary to design it based on the operation of the robot, dispatch control for the wagons, the capacity of the drying facility, and communication between these three elements.

Fuel efficiency was not dealt with in this study. Since the robot autonomously performs harvesting, homing, unloading, and restarting, fuel consumption for each operation and for the entire operation can be measured with respect to the algorithms. The homing scheduling can then also be explored in terms of fuel efficiency.

ACKNOWLEDGMENTS

This research is financially supported by the Scientific Research Grant (B) (No. 22380141) from Japan Society for the Promotion of Science, and the Research Grant from the Ministry of Agriculture, Forestry and Fisheries, in Japan.

The authors would like to express their appreciation to Dr. Rovira-Más, Professor of the Polytechnic University of Valencia, who helped to polish the manuscript, and to Mitsubishi Agricultural Machinery for providing the technical information about the base machine.

REFERENCES

Åstrand, B., & Baerveldt, A. J. (2002). An agricultural mobile robot with vision-based perception for mechanical weed control. Autonomous Robots, 13(1), 21–35.

Barawid, O. C., Jr., Mizushima, A., Ishii, K., & Noguchi, N. (2007). Development of an autonomous navigation system using a two-dimensional laser scanner in an orchard application. Biosystems Engineering, 96(2), 139–149.

Benson, E. R., Reid, J. F., & Zhang, Q. (2003). Machine vision-based guidance system for agricultural grain harvesters using cut-edge detection. Biosystems Engineering, 86(4), 389–398.

Billingsley, J., & Schoenfisch, M. (1997). The successful development of a vision guidance system for agriculture. Computers and Electronics in Agriculture, 16(2), 147–163.

Chateau, T., Debain, C., Collange, F., Trassoudaine, L., & Alizon, J. (2000). Automatic guidance of agricultural vehicles using a laser sensor. Computers and Electronics in Agriculture, 28(3), 243–257.

Coen, T., Vanrenterghem, A., Saeys, W., & De Baerdemaeker, J. (2008). Autopilot for a combine harvester. Computers and Electronics in Agriculture, 63(1), 57–64.

Cordesses, L., Cariou, C., & Berducat, M. (2000). Combine harvester control using real time kinematic GPS. Precision Agriculture, 2(2), 147–161.

Han, S., Zhang, Q., Ni, B., & Reid, J. F. (2004). A guidance directrix approach to vision-based vehicle guidance systems. Computers and Electronics in Agriculture, 43(3), 179–195.

Happich, G., Harmis, H. H., & Lang, T. (2009). Loading of agricultural trailers using a model-based method. Agricultural Engineering International: CIGR EJournal, 11, Manuscript 1187.

Iida, M., Uchida, R., Zhu, H., Suguri, M., Kurita, H., & Masuda, R. (2013). Path-following control of a head-feeding combine robot. Engineering in Agriculture, Environment and Food, 6(2), 61–67.

Kato, H., & Billinghurst, M. (1999). Marker tracking and HMD calibration for a video-based augmented reality conferencing system. Paper presented at the IWAR'99 Proceedings of the 2nd IEEE and ACM International Workshop on Augmented Reality. October, 1999, San Francisco, CA, USA.

Keicher, R., & Seufert, H. (2000). Automatic guidance for agricultural vehicles in Europe. Computers and Electronics in Agriculture, 25(1), 169–194.

Kise, M., Zhang, Q., & Rovira-Más, F. (2005). A stereovision-based crop row detection method for tractor-automated guidance. Biosystems Engineering, 90(4), 357–367.

Kise, M., Zhang, Q., & Noguchi, N. (2005). An obstacle identification algorithm for a laser range finder-based obstacle detector. Transactions of the ASAE, 48(3), 1269–1278.

Kurita, H. (2013). Autonomous unloading system for head-feeding combine robot. Unpublished Ph.D. thesis, Kyoto University. Available at http://www.kulib.kyoto-u.ac.jp/modules/search/index.php?content_id=16&ml_lang=en. Accessed November 22, 2014.

Kurita, H., Iida, M., & Suguri, M. (2012). Automation of unloading work -searching and detecting a grain container and proper positioning of a harvester's spout. Paper presented at the International Conference of Agricultural Engineering CIGR-AgEng. July, 2012, Valencia, Spain.

Kurita, H., Iida, M., Suguri, M., & Masuda, R. (2012). Application of image processing technology for unloading automation of robotic head-feeding combine harvester. Engineering in Agriculture, Environment and Food, 5(4), 146–151.

Kurita, H., Iida, M., Suguri, M., Masuda, R., & Cho, W. (2014). Efficient searching for grain storage container by combine robot. Engineering in Agriculture, Environment and Food, 7(3), 109–114.

Madsen, T. E., Kirk, K., & Blas, M. R. (2009). 3d camera for forager automation. Paper presented at the Land-technik AgEng. November, 2009, Hanover, Germany.

Nørremark, M., Griepentrog, H. W., Nielsen, J., & Søgaard, H. T. (2008). The development and assessment of the accuracy of an autonomous GPS-based system for intra-row mechanical weed control in row crops. Biosystems Engineering, 101(4), 396–410.

Nagasaka, Y., Saito, H., Tamaki, K., Seki, M., Kobayashi, K., & Taniwaki, K. (2009). An autonomous rice transplanter guided by global positioning system and inertial measurement unit. Journal of Field Robotics, 26(6–7), 537–548.

Nagasaka, Y., Umeda, N., Kanetai, Y., Taniwaki, K., & Sasaki, Y. (2004). Autonomous guidance for rice transplanting using global positioning and gyroscopes. Computers and Electronics in Agriculture, 43(3), 223–234.

Reid, J. F., Zhang, Q., Noguchi, N., & Dickson, M. (2000). Agricultural automatic guidance research in North America. Computers and Electronics in Agriculture, 25(1), 155–167.

Rovira-Más, F., Han, S., Wei, J., & Reid, J. F. (2007). Autonomous guidance of a corn harvester using stereo vision. Agricultural Engineering International: CIGR EJournal, 9, 1–13.

Stoll, A., & Kutzbach, H. D. (2000). Guidance of a forage harvester with GPS. Precision Agriculture, 2(3), 281–291.

Subramanian, V., Burks, T. F., & Arroyo, A. A. (2006). Development of machine vision and laser radar based autonomous vehicle guidance systems for citrus grove navigation. Computers and Electronics in Agriculture, 53(2), 130–143.

Torii, T. (2000). Research in autonomous agriculture vehicles in Japan. Computers and Electronics in Agriculture, 25(1), 133–153.

Wilson, J. N. (2000). Guidance of agricultural vehicles—A historical perspective. Computers and Electronics in Agriculture, 25(1), 3–9.

Xue, J., Zhang, L., & Grift, T. E. (2012). Variable field-of-view machine vision based row guidance of an agricultural robot. Computers and Electronics in Agriculture, 84, 85–91.